Beilstein-Institut

Experimental Standard Conditions of Enzyme Characterizations,
September 13th – 16th, 2009, Rüdesheim/Rhein, Germany

Parameterization of large-scale autonomous network models from time-series metabolite data

Klaus Mauch[1,*], **Ute Hofmann**[2], **Matthias Reuss**[3], **Klaus Maier**[1,3]

[1]Insilico Biotechnology AG, Nobelstrasse 15, 70569 Stuttgart, Germany

[2]Dr. Margarete Fischer-Bosch Institute of Clinical Pharmacology, Stuttgart and University of Tuebingen, Auerbachstrasse 112, 70376 Stuttgart, Germany

[3]Institute of Biochemical Engineering, University of Stuttgart, Allmandring 31, 70569 Stuttgart, Germany

E-Mail: *klaus.mauch@insilico-biotechnology.com

Received: 17th June 2010 / Published: 14th September 2010

Abstract

This contribution illustrates a framework for reconstructing and verifying large-scale kinetic metabolic network models in a semi-automated way. The experimental basis of this approach is provided by a stimulus response experiment. Parameterizing a large-scale kinetic network model then consists of three steps. In a first step, metabolic fluxes are identified. Subsequently, the dynamic network model is set-up automatically using canonical enzyme kinetics. In a third step, the kinetic parameters of the model are estimated from time-series metabolite data through integrating an evolutionary algorithm with a high-performance dynamic simulation platform. In this study, the time-series metabolite data were collected from HepG2 cells and analysed in the range of 0 to 180 minutes after depriving glucose from the culture medium. In total, more than 6 million simulation runs were performed. The *in silico* metabolite dynamics were in accordance with the experimental data.

Introduction

Kinetic network models allow for quantitative and systems-oriented predictions of cellular productivities, detoxification processes, and metabolic disorders like, for example, diabetes. Moreover, dynamic network models might eventually enable the personalized prognosis of drug actions and/or their persistency. However, to achieve a broad application and acceptance of dynamic *in silico* cells in the life science industries, a number of challenges need to be overcome. First and foremost, the model building currently is (too) slow and (too) costly. Next, the model representation and validation lack of standardized quality criteria, while setting up and managing large-scale network models lack of efficient computational tools. Finally, despite remarkable recent advances in metabolomics, acquiring adequate experimental data is still challenging, i. e. the issues of (fast) sampling and (reliable) quenching of single cells, cellular compartments and/or tissue are far from resolved.

In order to overcome the outlined challenges and to accelerate the reconstruction and identification of large-scale dynamic network models, the workflow shown in Figure 1 is proposed in this contribution.

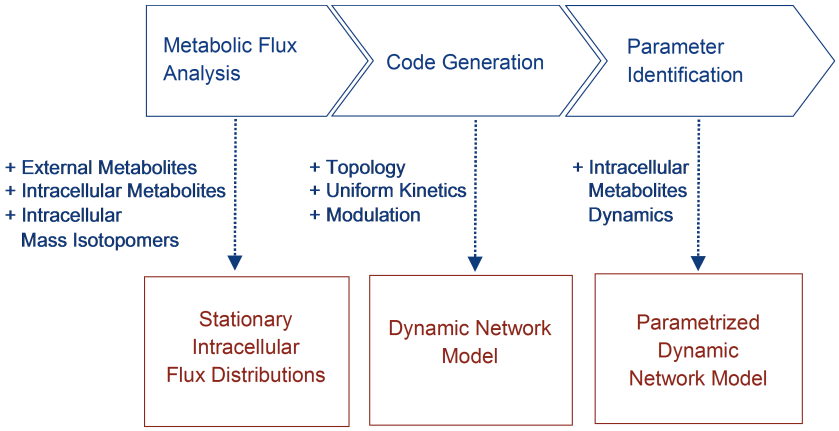

Figure 1. Workflow for parameterization of enzyme kinetics.

The complexity of the model parameterization process is effectively mitigated by breaking it down into a three-step procedure. In a first step, metabolic fluxes are identified. Subsequently, the dynamic network model is set-up automatically using canonical enzyme kinetics. In a third step, the kinetic parameters of the model are then estimated from time-series metabolite data. Identifying the network dynamics by referring to a physiologically relevant flux distribution confines both parameter range and network dynamics significantly. Moreover, the predictive quality of autonomous network models improves the closer predicted states to the experimentally observed reference state.

In the present study, a stimulus response experiment was performed using hepatoma cells. After growing HepG2 cells on a glucose-containing medium, the cells were incubated in fresh medium for two hours and then exposed to a medium lacking glucose. Metabolite time-series data were taken and analysed in the range of 0 to 180 minutes. The following sections will focus on (i) experimental methods, (ii) reconstruction of a large-scale autonomous network model, (iii) parameterization of the network model, and (iv) verification of *in silico* results.

Experimental Methods

HepG2 cells (ATCC® Number HB-8065™) were incubated at 37 °C in 6-well-plates in 5% CO_2 atmosphere. The cells were cultured in alanyl-glutamine-free William's medium E (PAN Biotech GmbH, Aidenbach, Germany) which was supplemented with penicillin (100 U/mL), streptomycin (100 mg/mL), and GibcoTM Insulin-Transferrin-Selenium (100X) supplement (Invitrogen, Karlsruhe, Germany). No fetal calf serum was added to the medium. The 6-well plates were shaken at 20 rpm throughout the experiment (Shaker DRS-12, ELMI, Riga, Latvia). The number of cells was determined using a Neubauer counting chamber. The intracellular flux map corresponding to this experimental setup was determined previously [1, 2]. The main flux was found to be the conversion of glucose to lactate. Thus, for designing an efficient stimulus response experiment, the glucose flux was considered as the most promising candidate for perturbing the central metabolism of the hepatoma cells. However, the cells were grown in a batch culture, and extracellular glucose was provided in excess. Therefore, it was concluded that an extracellular glucose pulse would not yield essential changes, whereas glucose deprivation was expected to trigger a substantial metabolic response.

Before depriving the cells of extracellular glucose, they were treated as described in [1]: The overnight medium was replaced with fresh culture medium, which was then exchanged with glucose-free medium after 2 h of equilibration. Extra- and intracellular samples were collected in triplicate directly before and after the stimulus, as well as 1, 2, 5, 10, 30, 60, 120, and 180 min after glucose deprivation. The sampling approach and the processing of the samples were done as described by Hofmann *et al.* [1].

The concentrations of alanine, serine, glucose, lactate, pyruvate, fumarate, malate, cis-aconitate, isocitrate, and citrate were determined by GC-MS as described in [1, 2]. After glucose deprivation, the extracellular glucose concentrations were determined in 10 µl of diluted (1:9 v/v) medium samples, the intracellular glucose concentrations before and after perturbation were determined in 5 and 50 µl of cell extract, respectively. Phosphoenolpyruvate, 3-phosphoglycerate, dihydroxyacetonphosphate, fructose-1,6-bisphosphate, glucose-6-phosphate, 6-phosphogluconate, sedoheptulose-7-phosphate, ribose-5-phosphate, and ribulose-5-phosphate were determined by LC-MS-MS as described by Hofmann *et al.* [1] with the following modifications: HPLC separation was performed at 20 °C on a Synergi Hydro-RP column

(150 x 2 mm, 4 µm; Phenomenex, Aschaffenburg, Germany) at a flow rate of 0.2 ml/min. The mobile phases consisted of (A) water with 10 mM tributylamine and 15 mM acetic acid, and (B) methanol. Gradient runs were programmed as follows: 100% A from 0 to 10 min, increase to 20% B to 25 min, remaining at 20% B to 30 min, increase to 35% B to 35 min, remaining at 35% B to 40 min, increase to 60% B to 45 min, increase to 90% B to 48 min remaining at 90% B to 50 min, then equilibrating with 100% A for 13 min. Precursor and product ions used for the quantification of glucose-6-phosphate, 6-phosphogluconate, ribose-5-phosphate, ribulose-5-phosphate, fructose-1,6-bisphosphate, and the internal standard mannitol-1-phosphate were as previously described [1] and for phosphoenolpyruvate: *m/z* 167/97, 139; 3- phosphoglycerate: *m/z* 185/97, 167; dihydroxyacetonphosphate: *m/z* 169/97 and sedoheptulose-7-phosphate: *m/z* 289/97, 199.

Nucleotide analysis was performed by reversed phase ion pair high performance liquid chromatography. The HPLC system (Agilent Technologies, Waldbronn, Germany) consisted of an Agilent 1200 series autosampler, an Agilent 1200 series Binary Pump SL, an Agilent 1200 series thermostated column compartment, and an Agilent 1200 series diode array detector set at 260 and 340 nm. The nucleotides were separated and quantified on an RP-C-18 column that was combined with a guard column (Supelcosil LC-18-T; 15 cm x 4.6 mm, 3 µm packing and Supelguard LC-18-T replacement cartridges, 2 cm; Supelco, Bellefonte, U.S.A.) at a flow rate of 1 ml/min. The mobile phases were (i) buffer A (0.1 M KH_2PO_4/K_2HPO_4, with 4 mM tetrabutylammonium sulfate and 0.5% methanol, ph 6.0) and (ii) solvent B (70% buffer A and 30% methanol, pH 7.2). The following gradient programs were implemented: 100% buffer A from 0 min to 3.5 min, increase to 100% B until 43.5 min, remaining at 100% B until 51 min, decrease to 100% A until 56 min and remaining at 100% A until 66 min.

Network Reconstruction

A kinetic network model was set up that includes the core metabolic pathways of hepatoma cells. The network model is based on a previously published isotopomer model that had been used for the estimation of intracellular fluxes from transient ^{13}C-labeling data [3] and accounts for 45 balanced compounds that are converted into each other by 49 reactions, including 5 transportation steps. The corresponding metabolic scheme is shown in Figure 2.

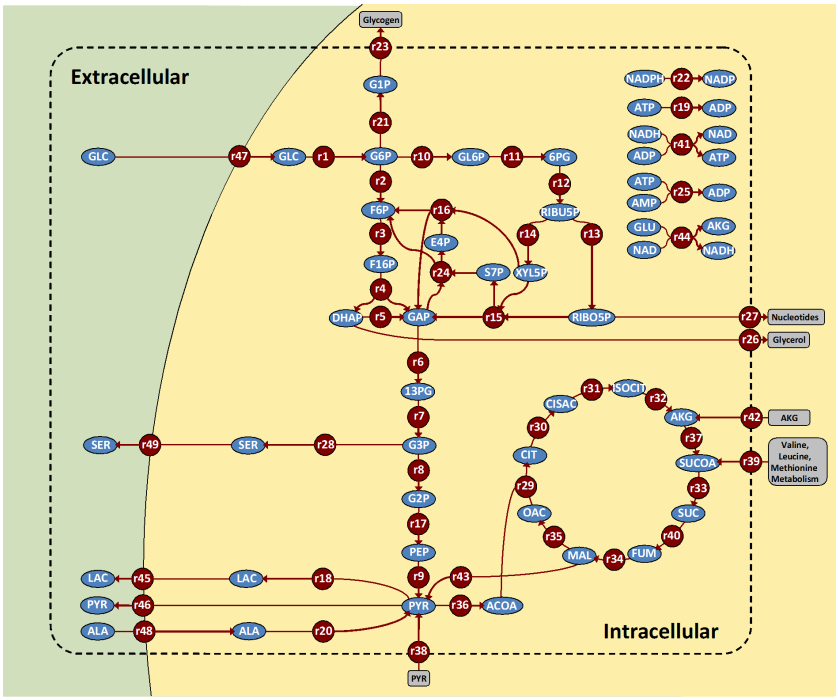

Figure 2. Metabolic network model of the hepatoma central metabolism. Extra- and intracellular metabolites are depicted with blue ellipses. Enzymatic reactions and transportation steps are indicated with red circles. Non-balanced compounds are shown within grey rounded rectangles. Directions of arrows reflect the direction of the steady state fluxes. The system boundary is indicated with a dashed line.

In the context of oxidative phosphorylation and the dynamic interplay of catabolism and anabolism, the cofactors NAD(H), NADP(H), ATP/ADP/AMP need to be taken into account by mass balances when analyzing the systems-level effect of the energy metabolism. The metabolic pathways under consideration contain 3 conserved moieties ($c_{amp}+c_{adp}+c_{atp}$ = -const; $c_{nadp}+c_{nadph}$ = const; $c_{nad}+c_{nadh}$ = const). The model comprises glycolysis (EMP), the pentose-phosphate pathway (PPP), and the tricarboxylic acid (TCA) cycle. In the cataplerotic section, the malic enzyme, which decarboxylates malate to pyruvate, is taken into account. Reduced NADH is regenerated in the lactate dehydrogenase and oxidative phosphorylation reactions. P/O ratios of 2.5 and 1.5 were assumed for NADH and succinate, respectively [4]. Based on experimental evidence [3], the metabolic state was assumed to be that of fed hepatic cells. Accordingly, no gluconeogenetic reactions were included. Exchange fluxes with the system boundary took into account glucose and alanine uptake, glycogen storage, the metabolism of glutamate, valine, leucine, and methionine, glycerol and nucleotide synthesis, as well as serine, lactate, and pyruvate excretion. In addition, reactions that

represented ATP and NADPH consumption relating to the basal metabolism were included. 31 regulatory effects (21 inhibitions and 10 activations) were found in a literature search [5] and included in the model (cf. Table 1).

Table 1. Activator and inhibitor influences. Regulatory influences and corresponding literature references. The modulator effects were included in the dynamic network model. In addition to these regulatory influences, the dynamic model did also account for substrate and product effects.

Enzyme Identifier	EC-Number	Activators	Inhibitors
glucokinase	2.7.1.2		F6P [23]
glucose-6-phosphate isomerase	5.3.1.9		6PG [24]
6-phosphofructokinase	2.7.1.11	AMP [25]	CIT [26]
fructose-bisphosphate aldolase	4.1.2.13		ADP, ATP, E4P, F6P, G1P, G6P, RIBO5P [27]
triose-phosphate isomerase	5.3.1.1		ATP [28]
glyceraldehyde-3-phosphate dehydrogenase	1.2.1.12		ADP, ATP [29]
phosphoglycerate kinase	2.7.2.3		AMP [30]
pyruvate kinase	2.7.1.40	G6P, F6P, G1P [31], F16P [32]	ALA [33]
glucose-6-phosphate dehydrogenase	1.1.1.49		ATP [34]
phosphoglucomutase	5.4.2.2		F16P [35]
UTP-glucose-1-phosphate uridylyltransferase	2.7.7.9		AMP [36]
alpha-ketoglutarate dehydrogenase	1.2.4.2	ADP [37]	ATP [37]
valine, isoleucine, methionine metabolism	-	NAD, AKG [38]	GLU, NADH [39]
isocitrate dehydrogenase	1.1.1.41	ADP [40]	
pyruvate dehydrogenase	1.2.4.1	AMP [41]	

The network model discriminated between 5 extracellular (glucose, lactate, serine, pyruvate, alanine) and 40 intracellular metabolites. The metabolic pathways neither contained dead-end metabolites nor strictly detailed balanced sub-networks [6]. Furthermore, all reactions were consistent with respect to mass conservation and redox state.

The following set of metabolite mass balances was set-up automatically to describe the time-dependent behaviour of a metabolic system:

$$\frac{d}{dt}\left(\frac{c}{c^0}\right) = \left(c^0\right)^{-1} \cdot N \cdot r \tag{1}$$

N denotes the stoichiometry matrix and **r** the rate vector. ($\mathbf{c}^0$) is a square diagonal matrix with reference concentrations on its main diagonal; $\left(\frac{c}{c^0}\right)$ denotes the normalized metabolite concentration vector.

Canonical linear-logarithmic (linlog) kinetics was automatically assigned for approximating the reaction rates in equation (1) [7 – 9]. The linlog formalism has been used for modelling *in vivo* kinetics and metabolic redesign [7]. Linlog kinetics was shown to have a good approximation quality and to need only relatively few parameters to be identified [10 – 12]. In linlog kinetics, all rate equations share a standardized mathematical format in which influences of metabolite and effector levels on reaction rates are taken into consideration by adding up logarithmic concentration terms. The standardized format is highly advantageous with a view to automating and speeding up the model set-up process. Besides, even for well-studied pathways of the central carbon metabolism it is often not the case that all kinetic mechanisms are known in detail [13, 14]. The matrix notation of the linlog rate equation is given by [7]

$$r = J^0 \cdot \left(\frac{e}{e^0}\right) \cdot \left(i + E_c^0 \cdot ln\left(\frac{c}{c^0}\right)\right) \tag{2}$$

in which $\mathbf{J}^0$ is the reference steady state flux distribution, $\left(\frac{e}{e^0}\right)$ is a diagonal matrix containing relative enzyme levels, and $\mathbf{i}$ is a vector of ones. $\mathbf{E}_c^0$ is a matrix whose entries are scaled elasticity coefficients ε_{ij} that describe the local effect of an infinitesimal change in concentration j on the rate of reaction i, i. e.

$$\varepsilon_{ij} = \left(\frac{\partial r_i}{\partial c_j}\right)^0 \cdot \frac{c_j^0}{r_i^0} \tag{3}$$

The ordinary differential equations (ODEs) were reformulated as differential algebraic equations (DAEs) to improve both the performance and stability of the numerical integrations, i. e. the conservation relations were solved algebraically. The DAE system was simulated with the linearly implicit differential algebraic solver «LIMEX» [15].

Network Parameterization from Time-Series Metabolite Data

Parameterizing a kinetic model requires the specification of a reference steady state, i. e. $\mathbf{J}^0$ and $\mathbf{c}^0$, and the corresponding kinetic parameters, i. e. $\mathbf{E}_c^0$. Each rate equation is assumed to be dependent on its substrate and product levels. In some instances additional effectors are taken into account;

The unknown elasticity coefficients and reference concentrations are identified by minimizing the differences between *in silico* model simulations and *in vivo* measurement data: The variance-weighted sum of squared residuals χ^2 between experimentally observed and simulated metabolite data, $\mathbf{c}^{\mathrm{m}}$ and $\mathbf{c}^{\mathrm{s}}$, is minimized according to

$$\min_{E_c^0,\, c^0} \; \chi^2\left(E_c^0,\, c^0\right) = (c^s - c^m)^T \cdot \Sigma_m^{-1} \cdot (c^s - c^m) \tag{4}$$

in which Σ_m is a diagonal matrix containing the measurement variances. An evolution strategy is applied for parameter fine-tuning that includes a self adapting mutation operator [16, 17].

The time-series metabolite data collected from HepG2 cell in the stimulus-response experiment were applied to parameterize the dynamic network model. Altogether, 174 scaled elasticities had to be estimated. Furthermore, 42 reference intermediate levels had to be identified (42 balanced compounds + 3 conserved moieties). The corresponding experimental data were available for 30 out of these. This means that in total 216 unknown parameters had to be specified in order to run a simulation. To enable a thorough exploration of the search space, the optimization runs were restarted after 100,000 evaluations of equation (4) using the best parameters currently available as starting values in the following iteration. Altogether, more than six million simulation runs were performed. On average, one simulation run took 0.2 seconds (Intel® Core2™ Quad CPU, 2.66 GHz, 4 GB RAM).

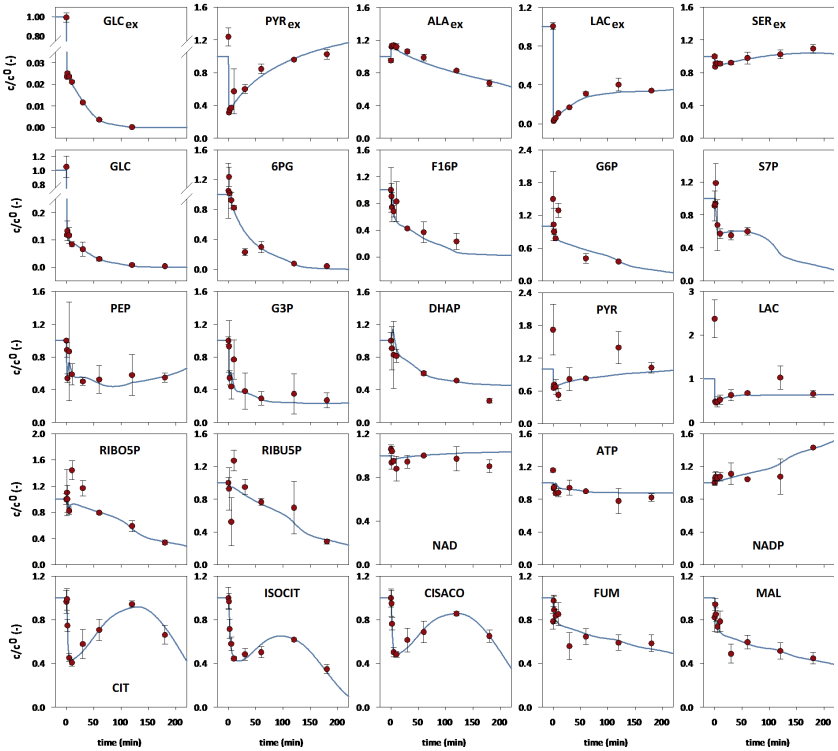

Figure 3. Experimentally determined (red circles) and simulated (blue solid lines) extra-/intracellular metabolite dynamics. The subscripts 'in' and 'ex' denote intracellular and extracellular metabolites, respectively. All concentrations were normalized with respect to the reference concentration directly before the stimulus. The error bars indicate standard deviations of the experimental data.

A total of 25 metabolite time courses were experimentally determined, of which 5 corresponded to extracellular metabolites and 20 to intracellular metabolites. The experimental data and the corresponding model simulations are summarized in Figure 3.

In vivo and *in silico* data were normalized with respect to the estimated reference values. It is worth noting that the perturbation triggered significant changes in the metabolite levels, and these changes provided important information about the underlying network dynamics. In general, the *in silico* metabolite dynamics were in accordance with the experimental data.

In Vivo and *In Silico* Metabolite Dynamics

After exchanging the glucose-containing culture medium with the glucose-free medium, the extracellular glucose level dropped drastically. The remaining extracellular glucose was consumed by the cells within a period of 120 min. The extracellular pyruvate and lactate levels also dropped considerably because of the medium exchange, but started to accumulate again. At the end of the experiment, i. e. after 180 min the pyruvate values were even slightly higher than the estimated initial level. Lactate did not reach 50 % of its initial value, which was the result of a decreasing lactate secretion rate. The initial efflux rate was twenty times higher for lactate than for pyruvate. This means that, in absolute terms, still more lactate than pyruvate was produced during the experiment. Extracellular alanine was consumed throughout the experiment, while extracellular serine accumulated. It is worth noting that besides the lack of glucose, the system was also perturbed as a result of the changes occurring in the extracellular pyruvate, lactate, alanine, and serine levels.

In accordance with the extracellular glucose levels, the intracellular glucose pool also decreased steeply. HepG2 cells have high GLUT2 transporter activities [18]. The GLUT2 transporter, which has a large K_m value, facilitates the diffusion of glucose into or out of the cells [19]. It can therefore be assumed that the steep decrease in the intracellular glucose pool was the result of the diffusion of intracellular glucose into the extracellular space. Consistently, the model simulations showed that the flux of glucose uptake was inversed immediately after the stimulus occurred. The intracellular glucose concentration further decreased and eventually converged to zero. With the exception of both phosphoenolpyruvate and pyruvate all other glycolytic metabolite levels decreased sharply immediately after the stimulus and continued to gradually decrease thereafter.

In the first 10 min of the experiment, the model simulations showed decreasing ribose-5-phosphate and ribulose-5-phosphate levels, followed by an increase, and then another decrease. Some discrepancy between the initial experimental data points and the simulations was observed for both metabolites, which could be an indication of a damped oscillation with rather high amplitude.

The first TCA cycle intermediate pools, i. e. citrate, cis-aconitate, and isocitrate, exhibited oscillatory dynamics. This was also found in the model simulations. It is interesting to note that three pairs of conjugate-complex eigenvalues were observed for the Jacobian matrix, which suggests that the system is capable of damped oscillations. The model simulations showed a non-oscillating decrease of fumarate and malate. There was some discrepancy between the simulated time courses for fumarate and malate and the experimentally observed concentrations after 30 min. However, the corresponding standard deviations were large.

The time courses of the experimentally determined cofactors NAD, ATP, and NADP only deviated slightly from their initial values. This means that despite the substantial changes in the metabolite levels in the central carbon metabolism, the homeostatic regulatory machinery of the hepatoma cells only allowed for small changes among the highly linked cofactors: ATP decreased slightly but remained at above 80 % of its steady state concentration, the NAD level increased only marginally, NADP increased a little more, reaching 143 % of its initial value. In contrast to these observations, distinct cofactor dynamics have been observed in similar stimulus response experiments in prokaryotes and yeast [20 – 22].

Perspectives

This contribution illustrates a framework for reconstructing and verifying kinetic metabolic network models in a semi-automated way. Since biochemical datasets like, for example, transcriptomic, proteomic, and metabolic data become increasingly available, the need as well as the potential for building predictive kinetic network models are gaining momentum. From a technical point of view, today's supercomputers and cloud computing environments allow for processing high-throughput experimental data in shorter time and at decreasing costs, thus enabling engineers and biochemists to use predictive kinetic network models as standard tool for decision making in areas like drug development and toxicity tests for the first time. From a more conceptual point of view, though, the application of large-scale predictive network models still faces a number of challenges. Fields such as (i) the coupling of signal transduction to metabolism, (ii) the systems-oriented breakdown of large-scale models into modules, and (iii) the integration of several modelling layers into concise representations of the biochemistry of whole organs and organisms are still not fully developed. Although enzyme kinetics form the building blocks of cellular dynamics, detailed kinetic information on many enzymes will probably remain rare and incomplete in the next decade. It is therefore anticipated that many questions at the systems-level will be answered through applying top-down/statistical approaches rather than through relying on bottom-up approaches.

Acknowledgements

Parts of this work were funded by HepatoSys (network detoxification), a systems biology funding initiative of the German Federal Ministry of Education and Research, and the Robert Bosch Foundation (Stuttgart, Germany). The excellent technical assistance of Sonja Seefried (Dr. Margarete Fischer-Bosch Institute of Clinical Pharmacology), Anja Niebel, and Gabriele Vacun (Institute of Biochemical Engineering, University of Stuttgart) is gratefully acknowledged. We also thank Jan G. Hengstler (Leibniz Research Centre for Working Environment and Human Factors at the University of Dortmund, Germany) for providing us with the HepG2 cell line.

References

[1] Hofmann, U. *et al.* (2008) Identification of metabolic fluxes in hepatic cells from transient 13C-labeling experiments: Part I. Experimental observations. *Biotechnol. Bioeng*. **100**:344 – 54.
doi: http://dx.doi.org/10.1002/bit.21747.

[2] Maier, K. *et al.* (2009) Quantification of statin effects on hepatic cholesterol synthesis by transient (13)C-flux analysis. *Metab. Eng.***11**:292 – 309.
doi: http://dx.doi.org/10.1016/j.ymben.2009.06.001.

[3] Maier, K. *et al.* (2008) Identification of metabolic fluxes in hepatic cells from transient 13C-labeling experiments: Part II. Flux estimation. *Biotechnol. Bioeng.* **100**:355 – 70.
doi: http://dx.doi.org/10.1002/bit.21746.

[4] Hinkle, P.C. (2005) P/O ratios of mitochondrial oxidative phosphorylation. *Biochim. Biophys. Acta* **1706**:1 – 11, Jan 7 2005.
doi: http://dx.doi.org/10.1016/j.bbabio.2004.09.004.

[5] Schomburg, I. *et al.* (2002) BRENDA, enzyme data and metabolic information. *Nucleic Acids Res.* **30**:47 – 9.
doi: http://dx.doi.org/10.1093/nar/30.1.47.

[6] Schuster, S. and Schuster, R. (1991) Detecting Strictly Detailed Balanced Subnetworks in Open Chemical-Reaction Networks. *Journal of Mathematical Chemistry* **6**:17 – 40.
doi: http://dx.doi.org/10.1007/BF01192571.

[7] Visser, D. and Heijnen, J.J. (2003) Dynamic simulation and metabolic re-design of a branched pathway using linlog kinetics. *Metab. Eng.* **5**:164 – 76.
doi: http://dx.doi.org/10.1016/S1096-7176(03)00025-9.

[8] Visser, D. *et al.* (2004) Optimal re-design of primary metabolism in *Escherichia coli* using linlog kinetics. *Metab. Eng.* **6**:378 – 90.
doi: http://dx.doi.org/10.1016/j.ymben.2004.07.001.

[9] Westerhoff, H.V. and van Dam, K. (1987) Thermodynamics and Control of Biological Free-Energy Transduction. Elsevier, Amsterdam.

[10] Heijnen, J.J. (2005) Approximative kinetic formats used in metabolic network modeling. *Biotechnol. Bioeng.* **91**:534 – 45.
doi: http://dx.doi.org/10.1002/bit.20558.

[11] Nikerel, I.E. *et al.* (2006) A method for estimation of elasticities in metabolic networks using steady state and dynamic metabolomics data and linlog kinetics. *BMC Bioinformatics* **7**: 540.
doi: http://dx.doi.org/10.1186/1471-2105-7-540.

[12] Hadlich, F., Noack, S., Wiechert, W. (2008) Translating biochemical network models between different kinetic formats. *Metab. Eng.* **11**(2):87 – 100.
doi: http://dx.doi.org/10.1016/j.ymben.2008.10.002.

[13] Hold, C. and Panke, S. (2009) Towards the engineering of *in vitro* systems. *J. R. Soc. Interface* **6**:507 – 521.
doi: http://dx.doi.org/10.1098/rsif.2009.0110.focus.

[14] Bulik, S. *et al.* (2009) Kinetic hybrid models composed of mechanistic and simplified enzymatic rate laws – a promising method for speeding up the kinetic modelling of complex metabolic networks. *FEBS J.* **276**:410 – 424.
doi: http://dx.doi.org/10.1111/j.1742-4658.2008.06784.x.

[15] Deuflard, P. *et al.* (1987) One Step and Extrapolation Methods for Differential-Algebraic Systems. *Numer. Math.* **51**:501 – 516.
doi: http://dx.doi.org/10.1007/BF01400352.

[16] Hansen, N. and Ostermeier, A. (2001) Completely derandomized self-adaption in evolutionary strategies. *Evolutionary Computation* **9**:159 – 195.
doi: http://dx.doi.org/10.1162/106365601750190398.

[17] Streichert, F. and Ulmer, H. (2005) JavaEvA: a Java based framework for Evolutionary Algorithms. *Technical Report* WSI-2005 – 06, Wilhelm-Schickard-Institut für Informatik (WSI), Center for Bioinformatics Tübingen (ZBIT), Eberhard-Karls-University Tübingen, Germany.

[18] Wu, C.H. *et al.* (2009) *In vitro* and *in vivo* study of phloretin-induced apoptosis in human liver cancer cells involving inhibition of type ii glucose transporter. *Int. J. Cancer* **124**:2210–2219.

[19] Thorens, B. (1996) Glucose transporters in the regulation of intestinal, renal, and liver glucose fluxes. *Am. J. Physiol.* **270**:541 – 553.

[20] Chassagnole, C., Noisommit-Rizzi, N., Schmid, J.W., Mauch, K., Reuss, M. (2002) Dynamic modeling of the central carbon metabolism of *Escherichia coli*. *Biotechnol. Bioeng.* **79**(1):53-73.
doi: 10.1002/bit.10288.

[21] Magnus, J.B. *et al.* (2006) Monitoring and modeling of the reaction dynamics in the valine/leucine synthesis pathway in *Corynebacterium glutamicum*. *Biotechnology Progress* **22**:1071-1083.

[22] Theobald, U., Mailinger, W., Baltes, M., Rizzi, M., Reuss, M. (1997) *In vivo* analysis of metabolic dynamics in *Saccharomyces cerevisiae*: *I. Experimental observations. Biotechnol. Bioeng*. **55**(2):305-316.
doi: http://dx.doi.org/10.1002/(SICI)1097-0290(19970720)55:2<305::AID-BIT8>3.0.CO;2-M.

[23] Veiga-da-Cunha, M. and Van Schaftingen, E. (2002) Identification of fructose 6-phosphate- and fructose 1-phosphate-binding residues in the regulatory protein of glucokinase. *J. Biol. Chem.* **277**:8466 – 73.
doi: http://dx.doi.org/10.1074/jbc.M105984200.

[24] Tsuboi, K.K. *et al.* (1971) Phosphoglucose isomerase from human erythrocyte. Preparation and properties. *J Biol. Chem.* **246**:7586 – 94.

[25] Berg, J. *et al.* (2002) Biochemistry. Fifth Edition, International Version, New York, W.H. Freeman & Co.

[26] Bloxham, D.P. and Lardy, H.A. (1973) Phosphofructokinase. In *The Enzymes*.Vol. 8, P. D. Boye (Ed.), 3rd ed. New York, Academic Press, pp. 239 – 278.

[27] Bais, R. *et al.* (1985) The purification and properties of human liver ketohexokinase. A role for ketohexokinase and fructose-bisphosphate aldolase in the metabolic production of oxalate from xylitol. *Biochem. J.* **230**:53 – 60.

[28] Gracy, R.W. (1975) Triosephosphate isomerase from human erythrocytes. *Methods Enzymol.* **41**:442 – 7.

[29] Gregus, Z. and Nemeti, B. (2005) The glycolytic enzyme glyceraldehyde-3-phosphate dehydrogenase works as an arsenate reductase in human red blood cells and rat liver cytosol. *Toxicol. Sci.* **85**:859 – 69.
doi: http://dx.doi.org/10.1093/toxsci/kfi158.

[30] Scopes, R.K. (1973) 3-Phosphoglycerate kinase. In *The Enzymes*. Vol. 8, P. D. Boyer (Ed.), 3 ed New York, Academic Press, pp. 335 – 351.

[31] Staal, G.E.J. *et al.* (1975) Human erythrocyte pyruvate kinase. *Methods Enzymol.* **42C**:182 – 186.
doi: http://dx.doi.org/10.1016/0076-6879(75)42113-9.

[32] Dombrauckas, J.D. *et al.* (2005) Structural basis for tumor pyruvate kinase M2 allosteric regulation and catalysis. *Biochemistry* **44**:9417 – 29.
doi: http://dx.doi.org/10.1021/bi0474923.

[33] Kahn, A. and Marie, J. (1982) Pyruvate kinases from human erythrocytes and liver. Methods Enzymol. **90** Pt E: 131 – 40.

[34] Cho, S.W. and Joshi, J.G. (1990) Characterization of glucose-6-phosphate dehydrogenase isozymes from human and pig brain. *Neuroscience* **38**:819 – 28.
doi: http://dx.doi.org/10.1016/0306-4522(90)90074-E.

[35] Fazi, A. *et al.* (1990) Purification and partial characterization of the phosphoglucomutase isozymes from human placenta. *Prep. Biochem.* **20**:219 – 240.
doi: http://dx.doi.org/10.1080/00327489008050198.

[36] Stryer, L. (1995) Biochemistry. W. H. Freeman and Company, Vol. 4.

[37] Gibson, G.E. *et al.* (2000) The alpha-ketoglutarate dehydrogenase complex in neurodegeneration. *Neurochem. Int.***36**:97 – 112.
doi: http://dx.doi.org/10.1016/S0197-0186(99)00114-X.

[38] Ogata, H. *et al.* (1999) KEGG: Kyoto Encyclopedia of Genes and Genomes. *Nucleic Acids Res.* **27**:29 – 34.

[39] Kanehisa, M. and Goto, S. (2000) KEGG: kyoto encyclopedia of genes and genomes. *Nucleic Acids Res.* **28**:27 – 30.
doi: http://dx.doi.org/10.1093/nar/28.1.27.

[40] Soundar, S. *et al.* (2003) Evaluation by mutagenesis of the importance of 3 arginines in alpha, beta, and gamma subunits of human NAD-dependent isocitrate dehydrogenase. *J. Biol. Chem.* **278**:52146 – 53.
doi: http://dx.doi.org/10.1074/jbc.M306178200.

[41] Lazo, P.A. and Sols, A. (1980) Pyruvate dehydrogenase complex of ascites tumour. Activation by AMP and other properties of potential significance in metabolic regulation. *Biochem. J.* **190**:705 – 10.